Wang, Luyao; Tan, Liping; Hu, Liqiu; Wang, Xiaoju; Koppolu, Rajesh; Tirri, Teija; van Bochove, Bas; Ihalainen, Petri; Sobhana Seleenmary Sobhanadhas, Liji; Seppälä, Jukka V.; Willför, Stefan; Toivakka, Martti; Xu, Chunlin

On Laccase-Catalyzed Polymerization of Biorefinery Lignin Fractions and Alignment of Lignin Nanoparticles on the Nanocellulose Surface via One-Pot Water-Phase Synthesis

Published in:
ACS Sustainable Chemistry and Engineering

DOI:
10.1021/acssuschemeng.1c01576

Published: 05/07/2021

Document Version
Publisher's PDF, also known as Version of record

ACS Sustainable Chemistry & Engineering

pubs.acs.org/journal/ascecg

Research Article

On Laccase-Catalyzed Polymerization of Biorefinery Lignin Fractions and Alignment of Lignin Nanoparticles on the Nanocellulose Surface *via* One-Pot Water-Phase Synthesis

Luyao Wang, Liping Tan, Liqiu Hu, Xiaoju Wang,* Rajesh Koppolu, Teija Tirri, Bas van Bochove, Petri Ihalainen, Liji Sobhana Seleenmary Sobhanadhas, Jukka V. Seppälä, Stefan Willför, Martti Toivakka, and Chunlin Xu*

Cite This: *ACS Sustainable Chem. Eng.* 2021, 9, 8770–8782

Read Online

ACCESS | Metrics & More | Article Recommendations | Supporting Information

ABSTRACT: Two series of well-defined lignin fractions derived from birch and spruce alkaline lignin (AL) by sequential solvent fractionation (*i*-PrOH-EtOH-MeOH) were engaged in a structure−property-application relationship study. The bacterial-derived alkaliphilic laccase (MetZyme) extensively catalyzed the oxidation and polymerization of AL fractions in an aqueous alkaline solution (pH 10). Lignin fractions with low molar mass reached a higher polymerization degree due to more phenolic-OH groups serving as reactive sites of oxidation and better lignin-laccase accessibility arose from a lower lignin condensation degree than the high molar mass ones. In comparison, AL fractions from spruce were found to be less reactive toward the laccase-catalyzed polymerization than those from birch, which was attributed to the much pronounced aryl-vinyl moieties' oxidation. Furthermore, *in situ* polymerization of birch AL fractions using microfibrillated cellulose as a structural template was conducted in an aqueous medium and a dispersion of nanocellulose with its fiber network evenly coated by aligned lignin nanoparticles was obtained. The present study not only provides fundamental insights on the laccase-assisted oxidation and polymerization of lignin but also presents a new perspective for valorizing lignin in biobased fiber products through green processing of solvent fractionation and enzymatic treatment.

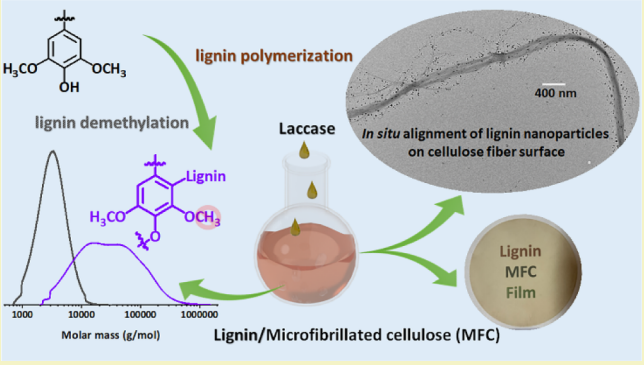

KEYWORDS: *alkaliphilic laccase, biomass, green chemistry, lignin polymerization, lignocellulosic nanocomposites*

INTRODUCTION

In plant cell walls, lignin is synthesized mainly from sinapyl alcohol (S), coniferyl alcohol (G), and *p*-coumaryl alcohol (H) monomers *via* an enzyme-initiated radical polymerization, resulting in an amorphous and three-dimensional polymer with both ether (*e.g.*, *β*-O-4′, 4-O-5′, and *α*-O-4′) and carbon−carbon (*e.g.*, *β*-1′, *β*−*β*′, and 5−5′) interunit linkages.[1] As the most abundant aromatic biopolymer on earth, lignin represents an important raw material for chemical, fuel, and polymer industries. Currently, approximately 70 million tons of technical lignins are produced annually around the world in the traditional pulping industry and carbohydrate-based biorefinery process (biofuel process).[2] Noteworthy, in the valorization of technical lignins, while substantial research is on the decomposition of lignin to aromatic monomers and oligomers,[3] the main industrial interests and developments are in the direct use and application of polymeric lignin.[4−6] The most intensively investigated application of polymeric lignin has been the use in traditional man-made thermosetting and thermoplastic structural materials.[6] To date, the new utilization trend is toward fabricating lignin-based materials with controlled architecture down to the micro- or nanoscale, such as micro- and nanoporous structures, micro- and nanocapsules, and nanoparticles.[5] In this scenario, polymerizing lignin using radical polymerization or a cross-linker (*e.g.*, epichlorohydrin, glutaraldehyde, *etc.*) is usually a necessary step to control the phase separation of lignin and fabricate micro- and nanostructured lignin-based materials.[7,8]

Oxidative enzymes, that is, laccases and peroxidases, are a promising biological and green tool for lignin substrate oxidation, decomposition, and polymerization.[9] As an eco-friendly valorization strategy, the enzymatic polymerization of lignin has been recently applied in the synthesis of new lignin-

Received: March 7, 2021
Revised: June 6, 2021
Published: June 21, 2021

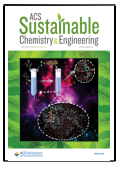

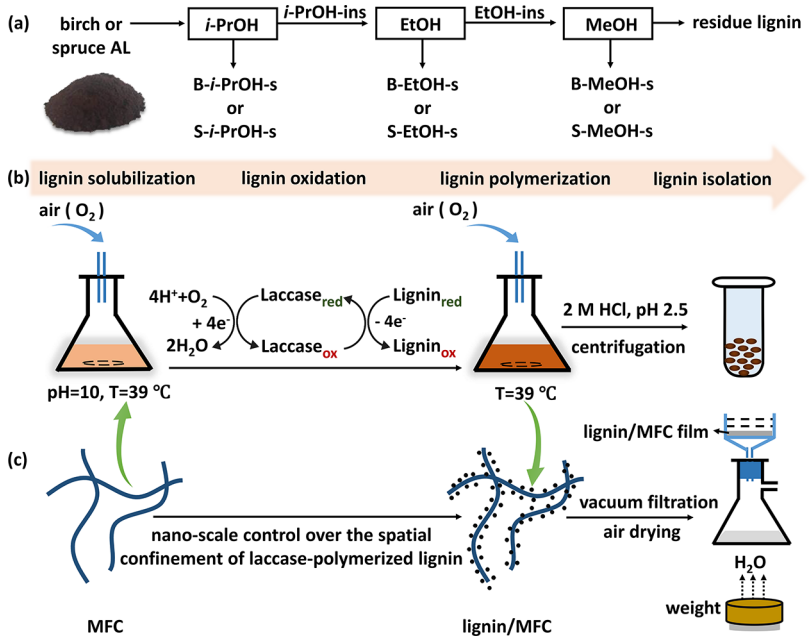

Figure 1. Representative schemes for the (a) preparation of well-defined AL fractions by sequential solvent extraction, (b) laccase-catalyzed polymerization of lignin fractions in an alkaline aqueous solution, and (c) *in situ* alignment of laccase-polymerized lignin on the surface of MFC as well as the fabrication of the lignin/MFC film.

based polymer materials, for example, fertilizer-controlled release systems,[10] enzymatically reinforced colloidal lignin nanoparticles, *etc.*[11,12] However, a lignin structure−property-performance correlation study has not yet been established in the existing body of the literature to correlate the lignin structural characteristics with laccase-assisted lignin polymerization performance, as well as to illustrate a more comprehensive picture for the lignin oxidative transformation. Meanwhile, the inherent heterogeneity of technical lignins, for example, chemical composition, molecular structure, and molar mass characteristics, still presents challenges for fundamental understanding and effective valorization of lignin in this context.[13] In a previous work, we reported on a lignin structure−property-application relationship of hardwood alkaline lignin (AL) that is isolated from a novel biorefinery process in the field of lignin-containing phenol-formaldehyde adhesive by solvent fractionation methodology.[14] The sequential solvent fractionation is suitable for elucidating the lignin structure−property-performance correlation as it can provide lignin fractions from the same parent lignin and endow lignin fractions with a reduced structural heterogeneity and more defined chemical characteristics, in terms of the molar mass, molar mass dispersity ($Đ_M$), functional group distribution, and lignin macromolecular structure.[15−17]

In the context of valorizing lignin with the aid of enzymatic catalysis, one of the major obstacles is the rather limited working pH range of fungal-derived laccases that are most available at an industrial-scale enzyme production. For example, *Melanocarpus albomyces* laccase (pH-range 5.0−7.5),[11] *Trametes hirsuta* laccase (pH-range 4.5−5.0),[11] and *Trametes versicolor* laccase (pH 5.0)[18] usually retain their activity under mesophilic and acidic reaction conditions, where technical lignin is hard to dissolve, except for the water-soluble lignosulfonates. Lignosulfonate is available as a highly sulfonated byproduct of the sulfite pulping process and accounts for only a marginal share of global technical lignin production.[6] Effective valorization strategies of other technical lignins, such as lignin from biorefinery processes, kraft lignin, soda lignin, *etc.*, are highly demanded. For the enzymatic treatment to these technical lignins, cosolvent systems as well as ionic liquids, have been strategically used to tackle with the solubility issue of lignins under the enzymatic working pH in water.[19−21] Those systems demonstrated good efficiencies but the utilization of these solvents still burdens the enzymatic treatment process with additional recycling need and potentially has a negative environmental impact in the end. In comparison to widely studied fungal laccases, the bacterial-derived laccase is known to have an extended working pH range, higher thermostability, and robustness in terms of the enzymatic activity and thus has attracted significant research attention.[22] Recently, enzymatic treatment of bulk industrial lignin *via* a new genetically evolved laccase (MetZyme) of bacterial origin was demonstrated under the extremely alkaline condition (pH 10.5), where lignin is soluble in water.[23] This bacterial-derived laccase is highlighted with great potential in upgrading lignin by increasing the number of functional hydroxyls through oxidative demethylation and depolymerization with the aid of laccase mediator.

With the present study, we first set the goal to investigate the correlations between lignin structural characteristics and laccase-assisted lignin oxidation/polymerization performance as well as to gain insights into the chemical transformation and oxidation pathways of lignin upon alkaliphilic laccase treatment. Accordingly, we proposed to adapt the sequential solvent fractionation to hardwood and softwood ALs in order to derive lignin fractions with well-defined characteristics. Then, those fractions were employed in the enzymatic oxidation and polymerization experiment under the lignin-soluble state (pH 10) aided by the treatment with MetZyme alkaliphilic laccase. Second, we hypothesized that the alkaliphilic laccase-catalyzed lignin polymerization in the aqueous single phase would allow a nanoscale control over the spatial confinement of lignin in cases of constructing nanocomposite materials of lignin with the other functional

https://doi.org/10.1021/acssuschemeng.1c01576
ACS Sustainable Chem. Eng. 2021, 9, 8770−8782

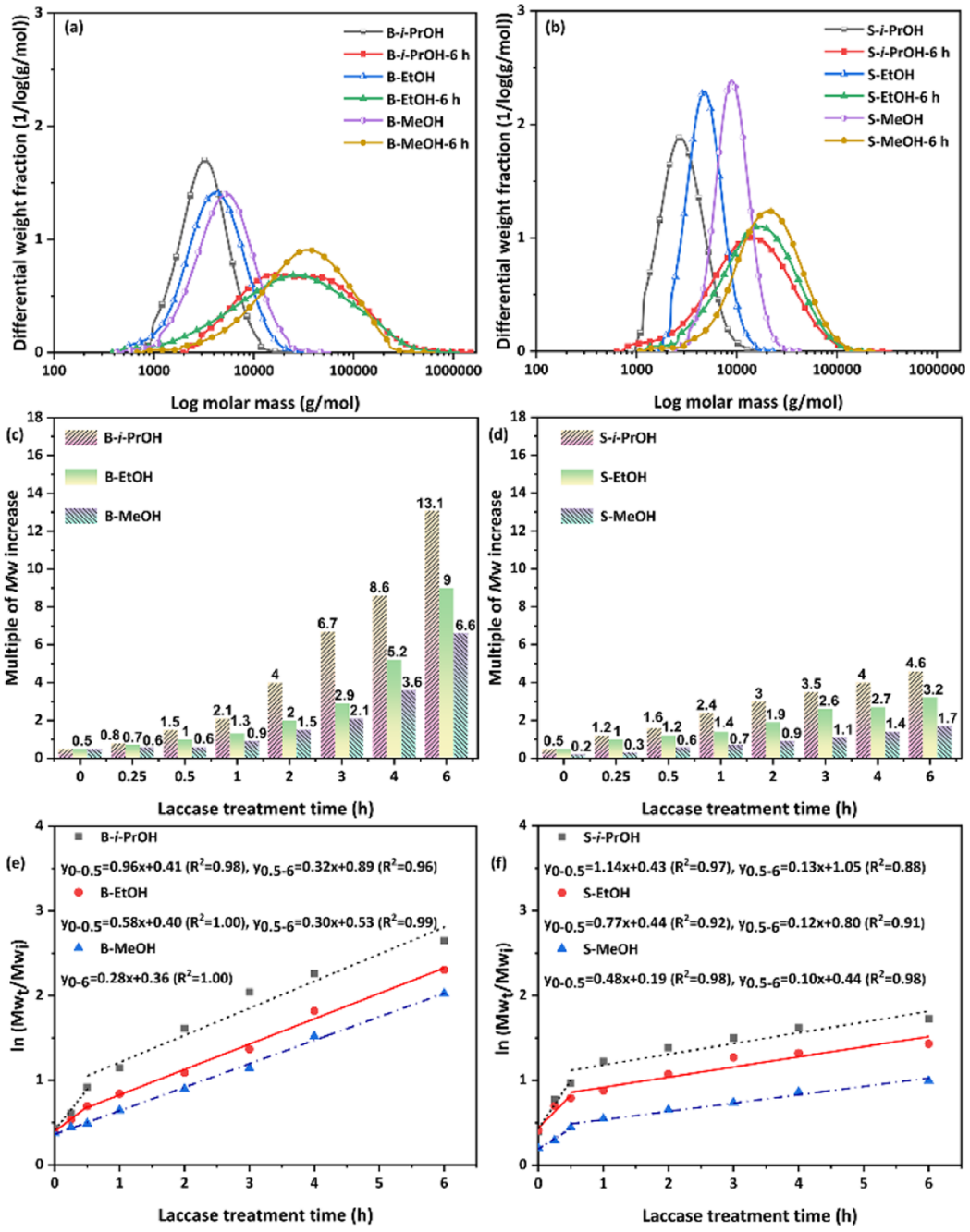

Figure 2. GPC chromatograms of birch (a) and spruce (b) AL fractions and their corresponding laccase-treated lignin demonstrating laccase-catalyzed lignin polymerization. Evolution of the M_W increase fold in (c,d) and the ln (M_{W_t}/M_{W_i}) *vs* laccase incubation time in (e,f). M_{Wt} represents M_W of lignin upon *t* hour's incubation while M_{W_i} represents the initial lignin molar mass.

nanomaterials, such as nanocellulose. In accordance with this hypothesis, we extended the study to *in situ* laccase polymerization of AL fractions with the suspended microfibrillated cellulose (MFC) present as a structural template for the polymerized lignin.

EXPERIMENTAL SECTION

Materials. Birch and spruce ALs were recovered by acid precipitation of spent liquor from the BLN biorefinery process, namely, pressurized hot water extraction and mild alkaline pulped process under the oxygen-starved condition.[24,25] The detailed lignin manufacturing and purification processes are available in Supporting Information. Birch or spruce AL was subdivided into three solvent-soluble lignin fractions by sequential dissolution in isopropyl alcohol (*i*-PrOH), ethanol (EtOH), and methanol (MeOH) according to the protocol established in our previous study (Figure 1a).[14] The industrial bacterial-derived alkaliphilic laccase MetZyme was supplied by MetGen Oy (Kaarina, Finland). The protein concentration was determined as 9.7 mg mL^{-1} using a Coomassie (Bradford) protein assay kit (ThermoFisher Scientific). The enzyme activity was determined as 357 U mL^{-1}, according to eq S1 (see details in Supporting Information).[26] MFC (0.4 wt % solid content) was prepared from dilute slurry of bleached kraft birch pulp (UPM, Finland) by mechanical refining pretreatment in a Valmet ProLanTM laboratory refiner and follow-up homogenization with a high-pressure homogenizer (A-100D, ATS Engineering Co., Ltd., China), where 2 passes at 200 bar and 10 passes at 1000 bar were used.

https://doi.org/10.1021/acssuschemeng.1c01576
ACS Sustainable Chem. Eng. 2021, 9, 8770−8782

Table 1. Extraction Yield, Molar Mass Characteristics, Functionality Distribution, and Lignin Backbone Compositions of Birch and Spruce ALs as well as Fractions Obtained by Sequential Solvent Fractionation

	birch AL fractions[14]				spruce AL fractions			
Properties	birch AL	*i*-PrOH	EtOH	MeOH	spruce AL	*i*-PrOH	EtOH	MeOH
extraction yield (wt %)	100	18	50	13	100	20	19	17
Molar Mass Characteristics								
M_W (g/mol)	7200	3700	4900	6200	17,600	3200	5100	9600
$Đ_M$	2.8	1.4	1.5	1.6	2.1	1.2	1.2	1.2
Lignin Hydroxyl Groups-Amount (mmol/g)[a]								
aliphatic-OH	1.1	1.0	1.1	1.4	1.7	1.3	1.6	1.7
C_5-substituted phenolic-OH	2.6	3.0	2.6	2.3	1.5	1.2	1.4	1.4
G phenolic-OH	0.7	0.8	0.8	0.7	1.8	2.2	1.8	1.6
total phenolic-OH	3.3	3.8	3.4	3.0	3.3	3.4	3.2	3.0
Lignin Interunit Linkages-Abundance (100 Ar)								
β-5′	---[b]	---	---	---	---	1.9	2.1	2.0
pinoresinol (β–β')	1.8	1.2	3.0	2.6	2.4	2.3	2.7	2.5
episinol (β–β')	---	---	---	---	---	1.0	1.1	0.8
secoisolariciresinol (β–β')	---	---	---	---	9.8	15.0	13.0	6.4
Aryl-vinyl Moieties-Abundance (100 Ar)								
stilbene β-5′	---	---	---	---	7.0	7.5	8.4	7.1
stilbene β-1′	---	---	---	---	3.6	4.7	1.5	0.9
aryl enol ether[c]	---	---	---	---	4.5	4.8	4.4	5.1
Lignin End Groups-Abundance (100 Ar)								
dihydro cinnamyl alcohol	---	---	---	---	1.5	3.6	5.7	4.2
aryl glycerol	3.3	3.0	4.1	2.8	6.4	4.7	6.5	3.7
S/G unit ratio[d]	3.1	3.3	3.0	2.5	0	0	0	0
DC[e]	21	27	34	40	74	47	64	75

[a]Quantified by ^{31}P NMR. [b]"---" denotes trace and beyond the HSQC detection limit. [c]Total amount of *cis*-enol ether and *trans*-enol ether. [d]Peak area ratio of S and G unit fragments in *Py*/GC–MS spectra. [e]Calculated by the combination of quantitative ^{13}C NMR and *Py*/GC–MS.[14]

Incubation of AL Fractions with Alkaliphilic Laccase. Lignin was solubilized at 10 mg mL^{-1} in sodium hydroxide (NaOH) solution (pH 10) for 3 h at room temperature. Laccase (MetZyme) was added to reach an enzyme activity of 1 U mg^{-1} of lignin. The solubilized lignin was incubated with laccase at 39 °C with ambient air (O_2) circulation under gentle agitation (400 rpm) (Figure 1b). After 0, 0.25, 0.5, 1, 2, 3, 4, and 6 h, 4 mL of the reacted sample was transferred to another tube and diluted 10 times in distilled water. The pH of the mixture was adjusted to 2.5 using hydrochloric acid (HCl, 2 M) and the mixture was centrifuged (8000 rpm, 10 min, 20 °C). The wet sediments of laccase-treated lignin were sufficiently frozen and then dried in a Martin CHRIST freeze-dryer (Alpha 1–4 LD Plus) under vacuum (0.067 mbar) above an ice condenser operating at −52 °C. Zero-hour laccase treatment was achieved by the lignin isolation right after the laccase was added to the reaction system.

Preparation of Lignin-Containing Cellulose Fibrils and Nanocomposite Films. MFC dispersion (0.4 wt %, 200 mL) was mixed with birch AL alkaline solution (pH 10, 10 mg mL^{-1}, dry mass ratio of MFC and lignin 19:1, 9:1, 5.7:1, and 4:1). The lignin/MFC mixture was equilibrated to 39 °C and pH 10 under 500 rpm stirring with aeration, and thereafter, laccase (1 U mg^{-1} of lignin) was introduced to initiate the lignin polymerization reaction. The reaction was continued for certain time (0.5, 1, and 2 h), and the lignin/MFC mixture was placed into a water bath at 90 °C for 15 min to inactive laccase and end reaction. Lignin/MFC nanocomposite films were fabricated using the vacuum filtration method as follows (Figure 1c): the laccase-treated lignin/MFC dispersion with 180 mg of dry content was diluted to a consistency of 0.2 wt % with alkaline water (pH 10, 0.5 M NaOH) and vacuum-filtered through a 0.2 μm Nylon membrane (diameter 90 mm) followed by film washing with distilled water until the pH of the filtrate is neutral. The wet film was peeled off and air-dried under 5 kg load at room temperature. The dried film was stored in a conditioned room with 50% relative humidity (RH) at 23 °C before further characterization.

Characterizations. Detailed information regarding instrumental setups and experimental procedures employed for lignin and lignin/MFC dispersion/film characterizations is given in Supporting Information.

RESULTS AND DISCUSSION

Characteristics of Birch and Spruce AL Fractions: Molar Mass, Hydroxyl Groups, and Constituent Patterns Revealed by Structural Analyses. Valorization of technical lignin demands lignin with a homogeneous feature in terms of molar mass dispersity. The technical lignins investigated here, birch and spruce ALs, had a respective weight-average molar mass (M_W) of 7200 and 17,600 g/mol and a $Đ_M$ of 2.8 and 2.1. A sequential solvent extraction strategy (*i*-PrOH-EtOH-MeOH) (Figure 1a) was carried out to address the heterogeneity of the starting technical lignins.[19] This provides two series of solvent-soluble lignin fractions with reduced $Đ_M$ (1.2–1.6), gradually increasing molar mass (Figure 2a,b), different functionality distributions, and lignin macromolecular backbone compositions at a total extraction yield of around 80 wt % from hardwood birch and 60 wt % from softwood spruce AL (Table 1). The amount of phenolic hydroxyl groups (phenolic-OH) available for initiating laccase-catalyzed lignin oxidation decreased gradually along the solvent fractionation sequence and correlated with increasing M_W and $Đ_M$ of the lignin fractions (Table 1). The constituent pattern, in terms of the aromatic units and interunit linkages, was also determined for the different AL fractions. The *i*-PrOH-soluble (*i*-PrOH-s) fraction from birch AL had the highest S/G ratio of 3.3, which decreased with increasing molar mass of the lignin fractions. The aromatic constituent pattern of spruce AL was exclusively G units (S/G = 0). The interunit linkages and

https://doi.org/10.1021/acssuschemeng.1c01576
ACS Sustainable Chem. Eng. 2021, 9, 8770–8782

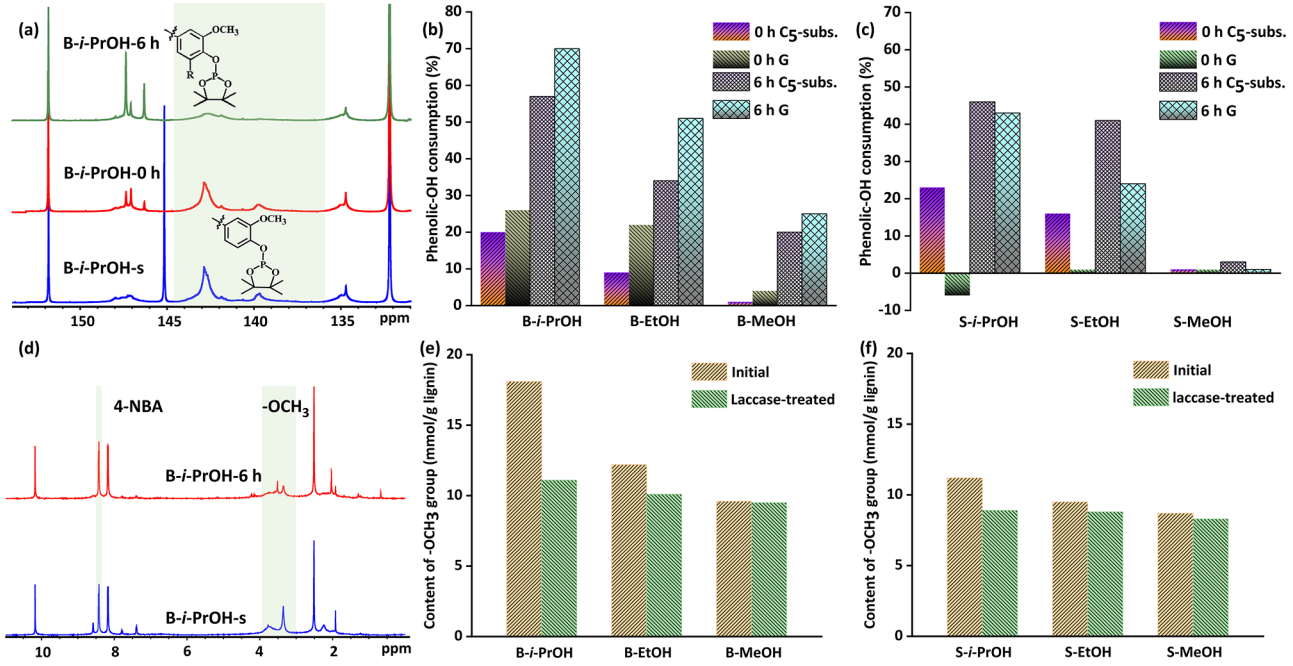

Figure 3. Laccase-catalyzed oxidation and demethylation of ALs. ^{31}P NMR of phosphitylated (a) B-*i*-PrOH-s and its corresponding laccase-treated lignin. The highlighted area indicates the integration range of phenolic-OH groups. Consumption percentage of phenolic-OH groups in laccase-treated birch (b) and spruce (c) AL fractions. ^{1}H NMR spectra of (d) laccase-treated B-*i*-PrOH-s after acetylation to demonstrate demethylation. The content of $-OCH_3$ groups in initial and laccase-treated (e) birch and (f) spruce lignin (6 h laccase incubation). The highlighted areas indicate the integration range of the internal standard [4-nitrobenzaldehyde (4-NBA)] at 8.4 ppm and $-OCH_3$ groups at 3.1−4.1 ppm, respectively.

substructures in the AL fractions were determined by combining the multiplicity-edited HSQC and quantitative ^{13}C NMR. The HSQC spectra and the ^{13}C-^{1}H correlation assignments of the identified interunit linkages and end groups in the birch/spruce AL substructures delineated in Figure S1 were assigned according to the previous literature and are reported in Figure S2 and Table S1.[27−29] It is observed that the native lignin interunit linkages (*β*-O-4′, *β*−*β*′, *β*-5′, and *β*-1′) were basically cleaved during the alkaline treatment of birch and spruce, especially for birch AL, in which only resinol structures (*β*−*β*′) survived under the alkaline condition. Meanwhile, aryl glycerol and aryl-vinyl moieties were concomitantly formed. Similar phenomena have been previously reported and rationalized on the basis of the alkaline pulping chemistry.[27,28,30] The aryl-vinyl structures, including stilbene and aryl enol ether, are of primary importance in understanding the reactivity of laccase-catalyzed lignin polymerization since they are very reactive toward oxidation, especially when oxygen (O_2) is involved.[27,30] It has to be noted that the aryl-vinyl moieties were detected in the HSQC spectra of spruce AL and its fractions in appreciable amounts and are enriched in low-molar-mass lignin fractions, whereas these structures were not detectable in birch ALs. This observation is consistent with earlier reported structural differences between alkaline eucalyptus and spruce lignins.[28] For the absence of the aryl enol ether structure in birch AL fractions, presumably, in hardwood lignin, most S units are patterned in etherified *β*-O-4′ motifs, which are cleaved leading to the accumulation of aryl glycerol structures under the alkaline condition.[31] In addition, Li *et al.* had also suggested that the phenolic *β*-O-4′ linkage of S units is more prone to undergo *β*-aryl ether bond cleavage with the concomitant formation of *β*−*β*′ linkage rather than transforming to the aryl enol ether structure than that between G units.[32] It is also clear that high-molar-mass lignin fractions showed a higher degree of condensation (DC, in % Ar) that emerges from aromatic ring substitution at C_2, C_5, and/or C_6 positions as compared to low-molar-mass counterparts (Table 1). This has ramifications for later laccase-catalyzed lignin polymerization where the chemical accessibility and steric hindrance of reactive sites for initiation of the reaction are important.

Laccase-Catalyzed Oxidation/Polymerization of AL Fractions under Alkaline Aqueous Conditions: Polymerization Kinetics and Lignin Structural Modifications. In order to probe the correlations between lignin characteristics and laccase-catalyzed lignin polymerization performance, the laccase-assisted lignin oxidation experiment was then carried out with the well-defined and well-characterized lignin fractions (Figure 1b). Gel permeation chromatography (GPC) analysis of the laccase-treated lignin clearly demonstrated that laccase treatment induced the polymerization of lignin to higher molar mass (Figure 2a,b), which is in line with the enzymatic lignin oxidation works reported by Munk *et al.* and Huber *et al.*[9,33] Detailed lignin molar mass data and GPC chromatograms are presented in Table S2 and Figure S3, respectively. Notably, the molar mass increase was higher in the low-molar-mass lignin fractions upon laccase treatment (Figure 2c,d), and the maximum molar mass was obtained for B-*i*-PrOH-6 h (52,000 g/mol). In addition, lignin fractions from birch AL were more efficient in molar mass polymerization than those from spruce AL, for example, 13.1-fold for B-*i*-PrOH-6 h compared with 4.6-fold for S-*i*-PrOH-6 h. The differences in the laccase-assisted lignin polymerization performance between birch and spruce AL fractions were also evident from the control experiment (under the same experimental conditions as B (S)-*i*-PrOH-6 h, only without laccase). More specifically, even without laccase addition, the S-*i*-PrOH-s fraction preserved a 0.8-fold molar mass increase,

https://doi.org/10.1021/acssuschemeng.1c01576
ACS Sustainable Chem. Eng. 2021, 9, 8770−8782

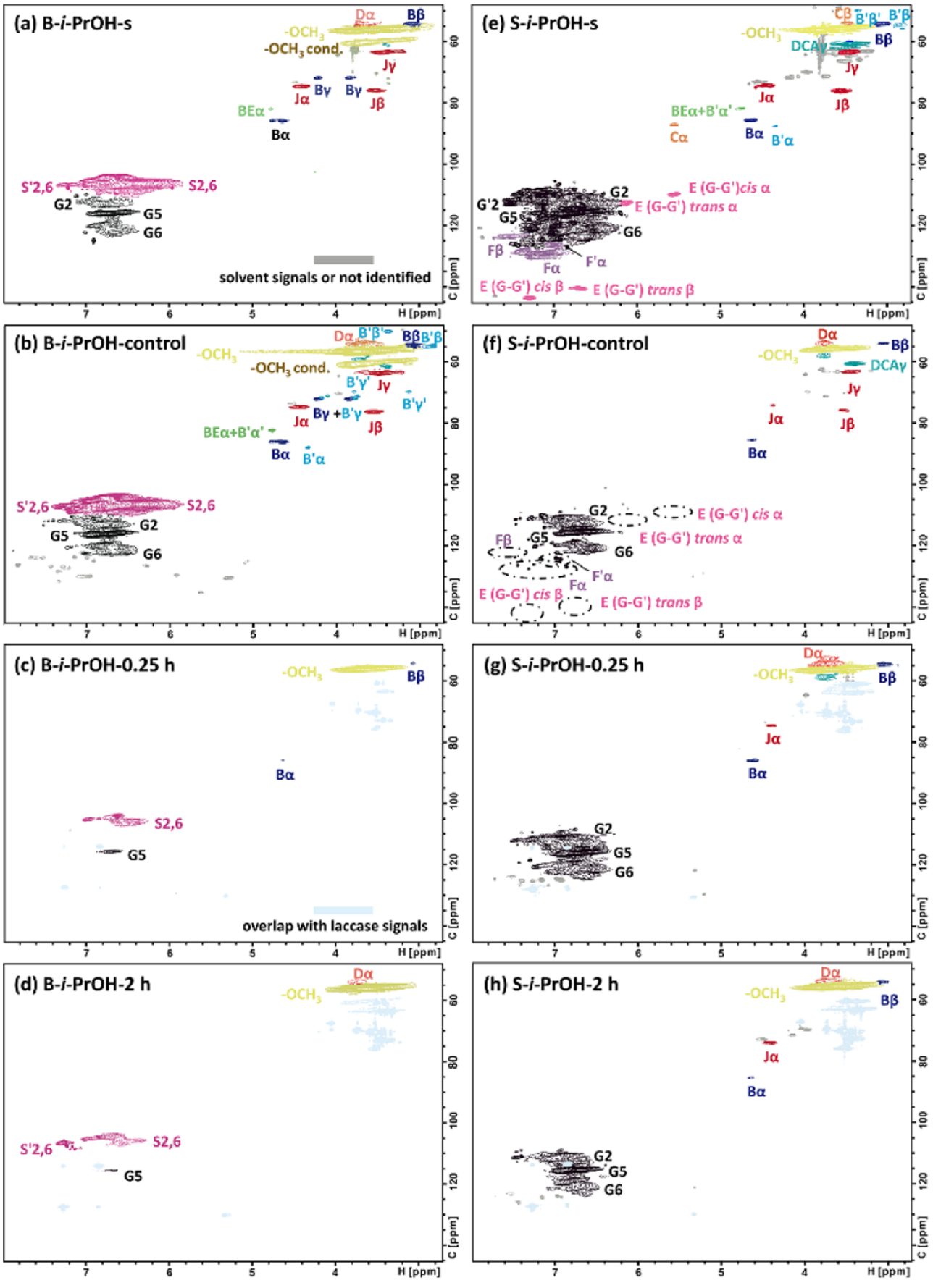

Figure 4. Structural changes to the birch and spruce ALs upon laccase treatment. HSQC NMR spectra of (a) B-*i*-PrOH-s, (b) B-*i*-PrOH-control, (c) B-*i*-PrOH-0.25 h, (d) B-*i*-PrOH-2 h, (e) S-*i*-PrOH-s, (f) S-*i*-PrOH-control, (g) S-*i*-PrOH-0.25 h, and (h) S-*i*-PrOH-2 h. (B) Pinoresinol

https://doi.org/10.1021/acssuschemeng.1c01576
ACS Sustainable Chem. Eng. 2021, 9, 8770−8782

Figure 4. continued

(β–β'), (B′) epiresinol (isomerous β–β' linkage), (B″) secoisolariciresinol (β–β'), (BE) benzyl ether lignin-carbohydrate complex linkages, (C) phenylcoumaran (β-5′), (D) α-5′ linked condensed structure, E (G–G′) *cis*-enol ether moieties linked with G units, E′ (G–G′) *trans*-enol ether moieties linked with G units, (F) stilbene moieties formed from β-5′ substructure, (F′) stilbene moieties formed from diphenylethane (β-1′) substructure, (S) S unit, (S′) α-oxidized S unit, (G) G unit, (H) H unit, (DCA) dihydro cinnamyl alcohol end group, and (J) aryl glycerol end group.

while negligible molar mass difference was shown in B-*i*-PrOH-s after the control experiment (Figure S4). To clearly elucidate the polymerization kinetics between different lignin fractions and lignin fractions from hardwood and softwood, the change in M_W was plotted *versus* laccase incubation time, and the slope, namely, the polymerization rate constant, was calculated by linear fitting (Figure 2e,f). The slope of the linear regression equation confirms once more an important notion that lignin fraction with initial low molar mass possessed a higher polymerization rate, especially within 0.5 h laccase incubation time.

In the absence of a redox mediator, the low redox potential of laccases usually prevents them from oxidizing nonphenolic lignin structures.[20] Therefore, the initiation of laccase-catalyzed lignin oxidation is believed to occur at phenolic-OH groups in the current work. In addition, it should be pointed out that only the phenolic-OH groups can be quantitatively monitored throughout the course of laccase treatment, as the phosphitylated laccase has severe interferences signals in the aliphatic hydroxyl groups (aliphatic-OH) and carboxylic acid areas of the ^{31}P NMR spectra (Figure S5). From Figure 3a–c, it is clear that the phenolic-OH groups in AL fractions considerably decreased upon laccase treatment, even at 0 h, which could be rationalized by the formation and coupling of laccase-induced phenoxy radicals within the lignin molecules.[9,34] As expected, AL fractions with low M_W and DC % as well as high content of phenolic-OH groups reached a higher molar mass polymerization degree (Figure 2c,d) and meanwhile consumed a higher percentage of phenolic-OH groups (Figure 3b,c, the integral values were listed in Table S3). This is attributed to higher reactivity of lignin as better chemical accessibility and/or lower steric hindrance in the corresponding laccase-catalyzed lignin oxidation/polymerization reaction. In addition, lignin fractions from birch AL consumed more phenolic-OH groups upon 6 h laccase treatment than the analogous fractions from spruce AL that have a similar molar mass and total amount of phenolic-OH groups. It seems to indicate that the presence of methoxyl groups ($-OCH_3$) on the constituent aromatic unit should account for the reactivity of the phenoxy radical toward oxidation assisted by laccase. As compared with fractions from spruce AL, birch AL fractions bear more S units with two *ortho*-methoxy substituents as revealed by pyrolysis-gas chromatography-mass spectrometry (*Py*/GC–MS) (Table 1). The $-OCH_3$ could favor the stabilization of phenoxy radicals by electron donation[35] and thus increase the phenolic-OH consumption, concomitantly with higher molar mass increase. S units in lignin are more active toward laccase oxidation than G units, which was also reported by Longe *et al.*[20] The content of $-OCH_3$ groups in laccase-polymerized lignins was also examined in Figure 3d–f. It suggests that oxidative demethylation of lignin occurred upon laccase treatment, which is in agreement with the results of MetZyme-assisted lignin oxidation reported in the literature.[23] Meanwhile, the observation of S-*i*-PrOH-0 h (2.31 mmol/g) contained more phenolic-OH groups from G units than S-*i*-PrOH-s (2.18 mmol/g) could be rationalized (Figure 3c, the ^{31}P spectra are shown in Figure S6), as the signal of phosphitylated phenolic-OH groups arose from demethylation is assigned to the phenolic G units in the ^{31}P NMR spectra.[36]

To gain further insights into the structural changes in lignin during the course of laccase treatment, the starting AL fractions (B-*i*-PrOH-s and S-*i*-PrOH-s) and laccase-treated counterparts were analyzed by HSQC NMR and are compared in Figure 4. The HSQC spectra of B (S)-*i*-PrOH-control samples (under the same experimental conditions as B (S)-*i*-PrOH-2 h, only without laccase) showed some differences compared to the B (S)-*i*-PrOH-s. The most significant difference is that alkali and air (O_2) conditions caused severe oxidation of aryl-vinyl moieties and oxidative condensation in S-*i*-PrOH-s, as revealed by the decreased intensity of the aromatic methine carbon (C_{Ar}-H) signals and the formation of (D) α-5′ condensed structures (Figure 4e,f). In contrast, the HSQC spectrum of B-*i*-PrOH-control is almost the same as that of B-*i*-PrOH-s, only (B′) epiresinol (isomerous β–β') structures were formed in the control experiment (Figure 4a,b). From the HSQC spectra of laccase-treated lignin, no newly formed radical-coupling linkages were detected in both of the polymerized B (S)-*i*-PrOH fractions, such as most common β-coupling linkages, as reactive precursors, for example, cinnamyl alcohol/aldehyde, *p*-coumarates, or ferulates, did not exist in the starting lignin fractions. For the B-*i*-PrOH-s fraction that was treated with laccase for only 0.25 h (Figure 4c), the side-chain signals of (B) β–β' and (J) aryl glycerol almost disappeared, and the C_{Ar}-H signals substantially diminished, particularly at $G_{2,6}$ and $S_{2,6}$ positions. When the laccase treatment of lignin was prolonged for 2 h, all the side-chain signals disappeared in the HSQC spectrum of B-*i*-PrOH-2 h. In addition to the cleavage of interunit linkages, the S units were C_α-oxidized, as revealed by the increased $S'_{2,6}$ signals (Figure 4d). Therefore, for laccase-treated birch AL fractions, it must be concluded that the lignin–lignin condensation/polymerization at aromatic C_2, C_5, and C_6 positions of B-*i*-PrOH-s was substantially induced by laccase-catalyzed oxidation under the alkaline condition. Previously, Dongre *et al.* have proposed a responsible mechanism, although it was investigated in the scenario of acid hydrolysis lignin: resonance effects of the electron pairs on $-OCH_3$ groups activate the C_2 and C_6 positions of lignin toward electrophilic substitution, thus could condense with the carbocation at CH-α that was formed from the cleavage of α-aryl ether under the acid condition.[37] In our case, the α-aryl ether linkages in (B and B′) β–β' and (C) β-5′ subunits were cleaved in the presence of air (O_2) and laccase. In addition, phenolic (J) aryl glycerol could undergo deprotonation with the concomitant formation of quinone methide intermediate under the alkaline condition, through which the CH-α position is electron-deficient and could react with electron-rich $G_{2,6}$, $S_{2,6}$, and G_5 positions. With electron resonance induced by the carbocation at CH-α, the C_2 and C_6 positions of lignin could also be electron-deficient, which allow the occurrence of both

https://doi.org/10.1021/acssuschemeng.1c01576
ACS Sustainable Chem. Eng. 2021, 9, 8770–8782

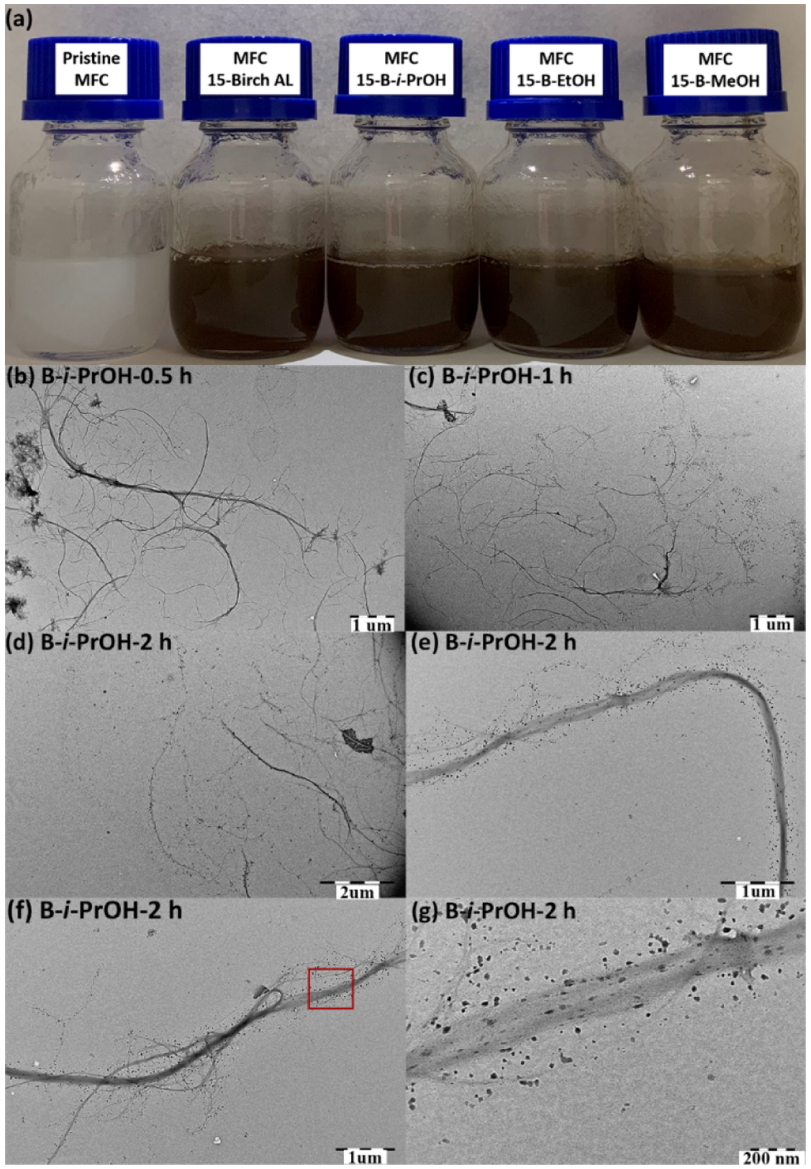

Figure 5. One-pot laccase-catalyzed lignin polymerization in the presence of MFC in the water phase. (a) Digital photographs of pristine MFC and lignin/MFC reaction mixture upon 2 h laccase treatment at 15 wt % loading of birch AL fractions showing good dispersity. TEM images of spatial confinement of the laccase-polymerized B-*i*-PrOH-s fraction (15 wt % loading) on the surface of MFC fibers with respect to variant reaction times, (b) 0.5 h, (c) 1 h, and (d–g) 2 h. (g) Zoom-in of the rectangular area in (f).

alkyl-aryl and aryl–aryl lignin condensation.[37] It is worth noting that the S-*i*-PrOH-s fraction exhibited rather prominent air (O_2)-induced oxidation of aryl-vinyl moieties (Figure 4e–h), while laccase-induced lignin–lignin condensation/polymerization at the aromatic ring was much less pronounced than that observed for the laccase-treated B-*i*-PrOH-s fraction. The differential response of spruce and birch ALs to the laccase-involved environment should be responsible for the difference in their molar mass increase.

With the aim of investigating how the air (O_2) oxidation environment assisted by laccase affects the relative molecular composition of ALs we investigated, the laccase-treated lignin fractions were analyzed by *Py*/GC–MS. The results, listed in Table S4, clearly demonstrate that the S/G unit ratio of birch AL fractions consecutively decreased upon laccase treatment, for example, decreased from 3.3 of B-*i*-PrOH-s to 2.9 of B-*i*-PrOH-0 h, further to 2.6 of B-*i*-PrOH-6 h. It indicates that lignin structural modifications, in terms of the constituent aromatic units, have occurred. The decrease in phenylpropane (C_6–C_3) pyrolysis compounds was also noticeable (Tables S5–10), as shown by the ratio between reduced side-chain (C_6–C_{0-2}) and full side-chain (C_6–C_3) lignin compounds, for example, increased from 8.4 of B-*i*-PrOH-s to 11.7 of B-*i*-PrOH-6 h or from 5.8 of S-*i*-PrOH-s to 7.3 of S-*i*-PrOH-6 h. The results are indicative of lignin unit side-chain cleavage, which agrees with the depolymerization of enzyme-treated lignin with C_α–C_β bond cleavage reported by the previous literature.[9,38] In addition, compared with spruce AL fractions, the content of catechol derivatives, including catechol, 3-methoxylcatechol, 3-methylcatechol, and 4-methylcatechol, significantly increased in laccase-treated birch AL fractions with respect to the starting lignin, except for the B-MeOH-s fraction (Table S4), which was coincided well with the laccase-assisted lignin demethylation results shown in Figure 3. In all, lignin oxidation, condensation/polymerization, side-chain fragmentation, and demethylation occurred simultaneously in

https://doi.org/10.1021/acssuschemeng.1c01576
ACS Sustainable Chem. Eng. 2021, 9, 8770–8782

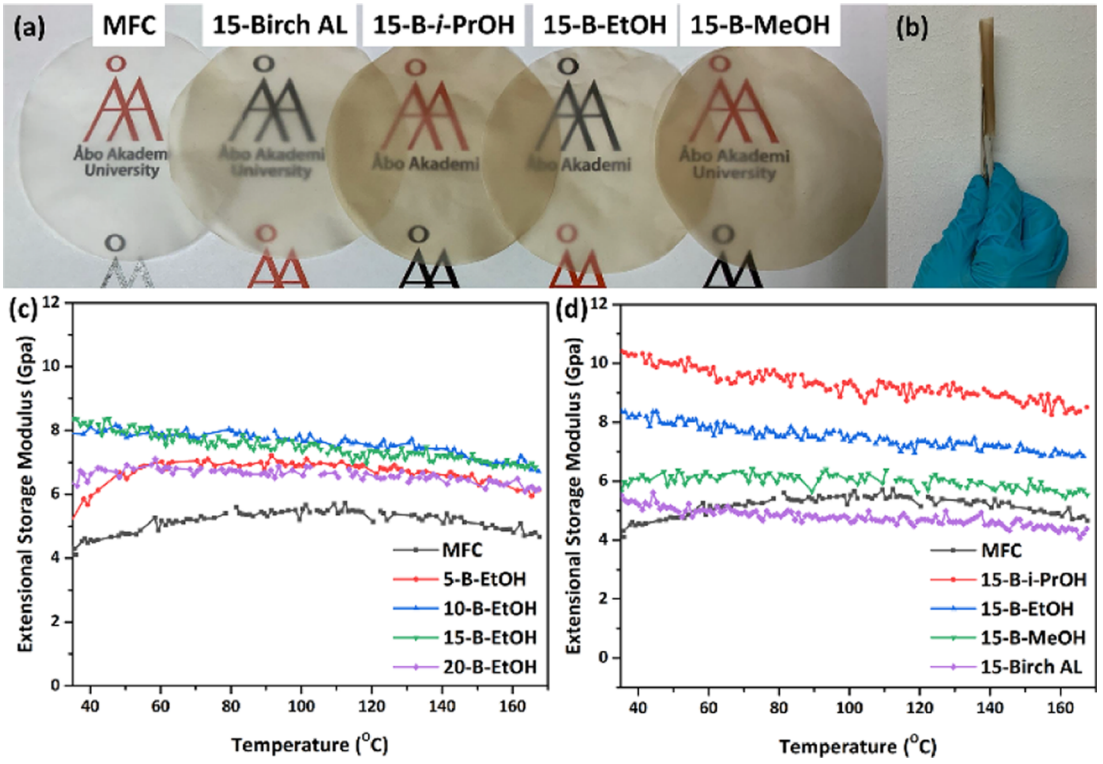

Figure 6. Photograph of the translucent lignin/MFC nanocomposite films (a) directly on top of the background and (b) rolling of the 15-B-*i*-PrOH film to demonstrate good mechanical robustness. The films prepared with 2 h laccase-treated birch AL fractions are termed *x*-lignin, with *x* presenting lignin dosage (wt %) in lignin/MFC dispersion. Effect of lignin dosage (c) and different birch AL fractions (d) on extensional E′ *vs* temperature curves of MFC and lignin/MFC nanocomposite films. Note: (a) the logo was reproduced with copyright permission from Åbo Akademi University.

the laccase-mediated alkaline aqueous medium, while lignin polymerization is much pronounced as revealed by the significant increase in molar mass. We also concluded that spruce AL fractions are more inert toward the laccase-mediated polymerization and structural modifications, while they are susceptible to air (O_2) oxidation.

Thermal Behaviors of the Laccase-Polymerized AL Fractions. The birch and spruce AL fractions as well as their laccase-polymerized products were analyzed by differential scanning calorimetry (DSC) and thermogravimetric analysis (TGA), in order to delineate key thermal parameters, such as glass transition temperature (T_g) and temperature value for the 50 wt % decomposition ($D_{1/2}$). As reported in Table S11, AL fractions showed increased T_g along the fractionation sequence, starting from 89 °C of B-*i*-PrOH-s to 162 °C of B-MeOH-s or from 78 °C of S-*i*-PrOH-s to 161 °C of S-MeOH-s, suggesting that the mobility of the lignin molecules was restrained by an increased lignin molar mass. As expected, all laccase-polymerized lignins exhibit higher T_g values than the initial counterparts, and B-*i*-PrOH-6 h lignin did not show T_g between 0 and 200 °C due to the high degree of polymerization. In comparison with initial AL fractions, the $D_{1/2}$ value and residue content obtained after complete decomposition increased in laccase-polymerized lignins, which endows the advantages of thermal stability and chemical tolerance to the laccase-polymerized lignins.

Alignment of Lignin Nanoparticles on the Cellulose Fiber Surface *via* One-Pot Laccase-Catalyzed Water-Phase Synthesis. Birch AL fractions are more active and were chosen to further investigate the laccase-catalyzed lignin polymerization process from a macro/nanoperspective. MFC dispersion (0.4 wt %) at alkaline pH 10 was used as the dissolution medium of birch AL fractions and *in situ* polymerization of lignin as confined along the MFC fibers was achieved by the addition of MetZyme into the water-phase synthesis (Figure 5a). First, the reaction duration was optimized in order to get well-controlled dimension and distribution of the polymerized lignin within the fiber network. The polymerization of B-*i*-PrOH-s in the MFC dispersion at 15 wt % dosage was monitored at durations of 0.5, 1, and 2 h by TEM imaging. At 0.5 h, it was seen that a few lignin nanoparticles had formed in the vicinity of the nanofibrils (Figure 5b). With extending the reaction duration to 1 and 2 h, the soluble lignin in the medium was further polymerized into a platelet-like morphology and was coated in alignment along the orientation of nanofibrils, as revealed in both TEM images (Figure 5c,d). An even distribution of polymerized lignin along the nanofibrils was more apparent for the B-*i*-PrOH-2 h sample. Surprisingly, the coating of lignin nanoparticles was even observed along tiny nanofibrils, as characteristically displayed in Figure 5e,f. The dimension of the polymerized lignin nanoparticles was no larger than 40 nm in a close observation, as shown in Figure 5g. With the polymerization duration set at 2 h and lignin dosage set at 15 wt %, the other two birch AL fractions, B-EtOH-s and B-MeOH-s, were further compared in the context of *in situ* polymerization along the MFC fibers. As shown in Figure S7, a similar scenario of polymerized lignin nanoparticles coated onto the nanofiber surface was further confirmed for the sample of B-EtOH-2 h. However, for the sample of B-MeOH-2 h, the polymerized lignin tended to form larger agglomerates and to appear as a thick coating on the fiber joints (Figure S8), which also

https://doi.org/10.1021/acssuschemeng.1c01576
ACS Sustainable Chem. Eng. 2021, 9, 8770−8782

Table 2. Mechanical Properties, Water Vapor Transmission Rate, Water Contact Angle, and Surface Free Energy of the Lignin/MFC Nanocomposite Films

	MFC	15-B-*i*-PrOH	15-B-EtOH	15-B-MeOH
density[a]	1.10 ± 0.05	1.17 ± 0.03	1.15 ± 0.03	1.25 ± 0.05
Young's modulus[a] (GPa)	3.03 ± 0.1	3.41 ± 0.3	3.16 ± 0.5	3.72 ± 0.4
tensile strength at break[a] (MPa)	81.66 ± 4.2	76.83 ± 3.9	63.66 ± 2.2	92.45 ± 8.5
strain at break[a] (%)	7.3 ± 1.3	6.5 ± 1.6	6.2 ± 1.0	6.4 ± 2.6
WVTR[a] ($g/m^2/day$)	212.2 ± 3	178.8 ± 4	202.2 ± 3	210.3 ± 10
WCA[a] (deg)	43.9 ± 1.5	50.4 ± 2.1	55.8 ± 0.2	46.9 ± 1.7
γ_p (mJ/m^2)[b]	31.6	29.0	24.6	28.3
γ_d (mJ/m^2)[c]	23.1	20.5	21.1	24.9
γ_γ (mJ/m^2)[d]	54.7	49.5	45.7	53.2

[a]The standard deviation from 3 to 6 parallel measurements is indicated. [b]SFE for dispersive components. [c]SFE for polar components. [d]SFE for dispersive plus polar components.

resulted in more severe fiber aggregation in the reaction medium. Hence, the morphology and distribution of the polymerized lignin within the MFC fiber network were inferred to be closely associated with the polymerization kinetics of the respective lignin fraction.

This one-pot, water-phase synthesis of polymerized lignin within the MFC nanofibril network ultimately facilitated a green and facile route for preparing the nanocomposite films of lignin and MFC *via* vacuum filtration. The nanocomposite films prepared from all three birch AL fractions had high transparency for film thicknesses in the range 30−40 μm and were mechanically robust (flexible), as seen in Figure 6a,b. The lignin content in the films deviated from the nominal lignin content of 15 wt % in the suspensions to a different extent according to the birch AL fractions, as revealed in the gravimetric analysis of lignin content in the filtrates from the vacuum filtration process (Table S12). Approximately, 11, 8, or 5 wt % lignin was retained in the nanocomposite films prepared from the polymerized lignin/MFC suspension with a 15 wt % dosage of B-*i*-PrOH-s, B-EtOH-s, or B-MeOH-s used in the *in situ* polymerization. This is conceivable as the polymerization degree decreased along the sequence of B-*i*-PrOH-s, B-EtOH-s, and B-MeOH-s.

In dynamic mechanical analysis (DMA), the extensional E′ of the prepared nanocomposite films was registered in a temperature range of 35−170 °C. E′ is an indication of the films' ability to store deformation energy in an elastic manner. Figure 6c compares the E′ of the nanocomposite films prepared from the polymerized B-EtOH-s fraction with variant lignin loading (5, 10, 15, or 20 wt %) upon 2 h laccase treatment with E′ of a pristine MFC film. All the nanocomposite films in this category displayed a higher E′ value than the MFC film. Furthermore, the E′ increased as the content of polymerized B-EtOH-s increased in gradient along the lignin loading from 5 to 10 and to 15 wt %. The nanocomposite film at 15 wt % loading of B-EtOH-s upon 2 h laccase treatment (15-B-EtOH) showed 8 GPa for the E′, which corresponded to a 60% enhancement to the E′ of the MFC film of 5 GPa. It is inferred that the morphologically homogenized coating of lignin nanoparticles along the MFC fibers formed in *in situ* polymerization ensures a superior dispersity of the polymerized lignin in the nanocomposite film. However, at 20 wt % loading of B-EtOH-s, the E′ of the obtained films dramatically decreased. This suggests that too high amounts of lignin can result in large lignin aggregates in the *in situ* polymerization that hinder the hydrogen-bonding interlocking among the MFC fibers. Another category of the nanocomposite films was prepared from all three sequential birch AL fractions at 15 wt % lignin loading and a polymerization duration of 2 h in *in situ* polymerization. In Figure 6d, their profiles of E′ *versus* temperature in DMA are compared to that of a pristine MFC film. Within the temperature window studied, the E′ of the nanocomposite films increased in the order of 15-B-MeOH, 15-B-EtOH, and 15-B-*i*-PrOH. The highest E′ was found for the film of 15-B-*i*-PrOH (around 10 GPa), whereas the film of 15-B-MeOH showed an E′ profile very close to that of the MFC film. This indicates that the thermomechanical property of the nanocomposite films in terms of E′ is strongly dependent on the degree of polymerization of the lignin fractions. It is interesting to note that the film prepared with the unfractioned birch AL with MFC through the *in situ* polymerization approach showed a deteriorated profile of E′ in comparison with that of the MFC film (Figure 6d). This confirms that the sequential solvent lignin fractionation is strategically significant in deriving high performance for this type of lignin-containing materials.

Mechanical properties of the nanocomposite films were further measured with tensile testing and the results are shown in Table 2. In general, when comparing to the pristine MFC film, the incorporation of *in situ*-polymerized lignin in the MFC network did not significantly alter Young's Modulus values. However, a slight decrease in the tensile strength at break was seen with films of both 15-B-*i*-PrOH and 15-B-EtOH. A large standard deviation to the tensile strength values was noticed among the sample groups of 15-B-MeOH nanocomposite films, which makes it difficult to draw a conclusion apart from the inhomogeneity of the obtained films from *in situ* polymerization of B-MeOH-s with the MFC fiber (Figure S8). To further study the interfacial interaction between the surface and solvent from a synergistic effect viewpoint, the contact angle on these nanocomposite films was measured using standard liquids, water and diiodomethane (see contact angle data in Table S13), as summarized in Table 2. The films of 15-B-*i*-PrOH and 15-B-EtOH showed slightly higher water contact angles (WCAs) of 50.5 and 55.8°, respectively, in comparison with 43.9° for the MFC films. The surface free energy (SFE) of 15-B-*i*-PrOH and 15-B-EtOH nanocomposite films decreased to 49.5 and 45.7 mJ/m^2 in comparison with 54.7 mJ/m^2 for the MFC film. The nanocomposite films of 15-B-MeOH had a similar WCA (46.9°) and SFE (53.2 mJ/m^2) with the MFC film. This is also in line with the inhomogeneity of the nanocomposite film of this kind. Furthermore, in the water vapor permeation tests evaluated under conditions of 23 °C and RH of 50%, the

https://doi.org/10.1021/acssuschemeng.1c01576
ACS Sustainable Chem. Eng. 2021, 9, 8770−8782

nanocomposite films of 15-B-*i*-PrOH and 15-B-EtOH showed a slightly lower water vapor transmission rate (WVTR) of 179 and 202 g/m^2/day, in comparison with 212 g/m^2/day for the MFC film. This indicates once more a decreased water vapor solubility in these polymerized lignin/MFC films. Not surprisingly, the films of 15-B-MeOH did not show any improvement on the water vapor barrier as judged by the WVTR value in Table 2.

Among the recent state-of-the-art studies on the preparation of lignin-containing nanocellulose films, two major categories of processing strategies have been intensively studied, that is, either preserving the residual lignin in biomass pretreatments or mixing isolated lignin in various formats in the cellulose nanofibril (CNF) matrix. In the former category, the preserved residual lignin was beneficial to the defibrillation when treating bagasse fibers with improved nanofibril yield but reduced energy consumption[39] and it also significantly improved the wet tensile strength of the obtained composite film prepared from tobacco stalk.[40] In the latter category where the currently reported approach falls in, the importance of finely tuning the interfacial interactions to result in efficient integration of lignin in the CNF matrix has been highlighted. In cases that lignin with different charge groups was directly mixed in as nanoparticles[41] or lignin was *in situ*-precipitated on the nanofibril matrix in nucleation-and-growth fashion *via* a solvent shifting method,[42] the mechanical properties and surface wettability of the as-fabricated nanocellulose films largely varied, mainly dictated by the interfacial interactions resulted in the matrix. Analogously, the enzymatically polymerizing the soluble alkaline lignin fraction with MFC as a structural template *in situ* has allowed a well-controlled spatial confinement of polymerized lignin on the nanoscale in the nanocellulose fiber network. As strongly inferred by the mechanical properties, wettability, and water vapor transmission of the nanocomposite films as-fabricated, this one-pot, water-phase synthesis has potential in development of functional biobased packaging taking the advantages of the holistic processing approach being green and sustainable.

CONCLUSIONS

The bacterial-derived alkaliphilic laccase (MetZyme) significantly catalyzed the oxidation and polymerization of birch AL fractions under mild conditions, for example, 13.1-fold molar mass increase for the B-*i*-PrOH-s fraction after 6 h of treatment. Compared with birch AL fractions, spruce AL fractions exhibited rather prominent oxidation of aryl-vinyl moieties even without the laccase mediation and that also resulted in less-pronounced polymerization of lignin substrates, for example, only 4.6-fold molar mass increase for the S-*i*-PrOH-s fraction. Coupling and resonance of laccase-induced phenoxy radicals, cleavage of α-aryl ether interunit linkages, such as β–β' and β-5′, and electron-donating effect of $-OCH_3$ groups substantially induced the lignin–lignin condensation/polymerization at C_2, C_5, and C_6 positions. In addition, lignin demethylation and benzylic oxidation also occurred upon laccase treatment, highlighting the complexity of the chemo-enzymatic interactions. The correlation between lignin structural characteristics and performance of the alkaliphilic laccase-mediated lignin polymerization was established based on molar mass, amount of phenolic-OH groups, and DC %. Strategically, *in situ* laccase-catalyzed polymerization of the B-*i*-PrOH-s fraction with the presence of MFC fibers in an aqueous single-phase medium allows a localized and homogeneous coating of lignin nanoparticles with a dimension less than 40 nm along the MFC fiber network. This green synthetic route ensures a superior dispersity of the polymerized lignin in the obtained nanocomposite films.

ASSOCIATED CONTENT

Supporting Information

The Supporting Information is available free of charge at https://pubs.acs.org/doi/10.1021/acssuschemeng.1c01576.

> Lignin manufacturing and purification process, enzyme activity and protein concentration assay, instrumental setups and detailed experimental procedures for lignin and MFC/lignin dispersion/film characterizations, main lignin structures detected by HSQC, assignment of the main $^{13}C-^{1}H$ correlation signals, HSQC spectra of birch and spruce AL, ^{31}P NMR of laccase and laccase-treated S-*i*-PrOH, GPC chromatograms of laccase-treated lignins, tables of lignin molar mass, *Py*/GC–MS, DSC, and TGA data, TEM images of MFC with *in situ* laccase-polymerized B-EtOH-s and B-MeOH-s fractions, lignin dry content of the film, and contact angle of diiodomethane on lignin/MFC films (PDF)

AUTHOR INFORMATION

Corresponding Authors

Xiaoju Wang − *Laboratory of Natural Materials Technology, Åbo Akademi University, Turku FI-20500, Finland*; Email: Xiaoju.Wang@abo.fi

Chunlin Xu − *Laboratory of Natural Materials Technology, Åbo Akademi University, Turku FI-20500, Finland*; orcid.org/0000-0003-1860-9669; Email: Chunlin.Xu@abo.fi

Authors

Luyao Wang − *Laboratory of Natural Materials Technology, Åbo Akademi University, Turku FI-20500, Finland*

Liping Tan − *Laboratory of Natural Materials Technology, Åbo Akademi University, Turku FI-20500, Finland; State Key Laboratory of Biobased Material and Green Papermaking, Qilu University of Technology, Shandong Academy of Sciences, Jinan 250353, China*

Liqiu Hu − *Laboratory of Natural Materials Technology, Åbo Akademi University, Turku FI-20500, Finland*

Rajesh Koppolu − *Laboratory of Natural Materials Technology, Åbo Akademi University, Turku FI-20500, Finland*; orcid.org/0000-0002-0966-7587

Teija Tirri − *Laboratory of Molecular Science and Engineering, Åbo Akademi University, Turku FI-20500, Finland*

Bas van Bochove − *Research Group of Polymer Technology, Department of Chemical and Metallurgical Engineering, Aalto University, Espoo FI-02150, Finland*

Petri Ihalainen − *MetGen Oy, Kaarina FI-20780, Finland*

Liji Sobhana Seleenmary Sobhanadhas − *MetGen Oy, Kaarina FI-20780, Finland*

Jukka V. Seppälä − *Research Group of Polymer Technology, Department of Chemical and Metallurgical Engineering, Aalto University, Espoo FI-02150, Finland*; orcid.org/0000-0001-7943-3121

Stefan Willför − *Laboratory of Natural Materials Technology, Åbo Akademi University, Turku FI-20500, Finland*

Martti Toivakka − *Laboratory of Natural Materials Technology, Åbo Akademi University, Turku FI-20500, Finland*

Complete contact information is available at: https://pubs.acs.org/10.1021/acssuschemeng.1c01576

Author Contributions

L.W., L.T., and L.H. equally contributed to the data collection, analysis, and interpretation: L.T. initially validated the laccase-polymerization parameters during her research visit at Åbo Akademi University; L.W. carried out the lignin fractionation as well as the multiple-instrumental characterizations on the polymerized samples; L.H. carried out the laboratory work on the *in situ* polymerization of lignin with nanocellulose and further film-making and its characterizations. L.W. and X.W. drafted the manuscript together. R.K. contributed to the mechanical analysis of the film samples. T.T. and B.v.B. contributed to the thermal analysis to the lignin fractions and their polymerized counterparts. P.I. and L.S. have provided the enzyme and relevant application protocols and contributed to the manuscript revision. S.W., M.T., and J.S. provided critical revision to the manuscript. C.X. and X.W. are the main principle scientists who conceptualized and cosupervised the work. The manuscript has been approved by all the coauthors for submission.

Notes

The authors declare no competing financial interest.

■ ACKNOWLEDGMENTS

Business Finland Project (43674/31/2020) is acknowledged for the research funding to the current work. L.T. would like to thank the financial support to conduct research mobility at Åbo Akademi University (ÅAU) provided by Johan Gadolin Scholar mobility funding programme. Both L.W. and L.H. would like to acknowledge the financial support from the China Scholarship Council (Student ID 201804910639 for L.W. and Student ID 201908120107 for L.H.) to their doctoral study at ÅAU, Finland. Jarl Hemming and Dr. Annika Smeds are greatly acknowledged on their help with GPC and *Py*/GC−MS analysis. Qingbo Wang is thanked for his work with DMA measurements. Dr. Andrey Pranovich is thanked for discussing while initializing the project. CH-Bioforce Oy (Espoo, Finland) is thanked for providing birch and spruce ALs. This work is also part of activities within the Johan Gadolin Process Chemistry Centre (PCC) at ÅAU. This work also made use of Aalto University Bioeconomy Facilities.

■ REFERENCES

(1) Ralph, J.; Lapierre, C.; Boerjan, W. Lignin Structure and Its Engineering. *Curr. Opin. Biotechnol.* **2019**, *56*, 240−249.
(2) Berlin, A.; Balakshin, M. Industrial Lignins: Analysis, Properties, and Applications. *Bioenergy Res.: Adv. Appl.* **2014**, 315−336.
(3) Rinaldi, R.; Jastrzebski, R.; Clough, M. T.; Ralph, J.; Kennema, M.; Bruijnincx, P. C. A.; Weckhuysen, B. M. Paving the Way for Lignin Valorisation: Recent Advances in Bioengineering, Biorefining and Catalysis. *Angew. Chem., Int. Ed.* **2016**, *55*, 8164−8215.
(4) Balakshin, M. Y.; Capanema, E. A.; Sulaeva, I.; Schlee, P.; Huang, Z.; Feng, M.; Borghei, M.; Rojas, O. J.; Potthast, A.; Rosenau, T. New Opportunities in the Valorization of Technical Lignins. *ChemSusChem* **2021**, *14*, 1016−1036.
(5) Duval, A.; Lawoko, M. A Review on Lignin-Based Polymeric, Micro- and Nano-Structured Materials. *React. Funct. Polym.* **2014**, *85*, 78−96.
(6) Glasser, W. G. About Making Lignin Great Again-Some Lessons From the Past. *Front. Chem.* **2019**, *7*, 1−17.
(7) Saidane, D.; Barbe, J.-C.; Birot, M.; Deleuze, H. Preparation of Functionalized Kraft Lignin Beads. *J. Appl. Polym. Sci.* **2010**, *116*, 1184−1189.
(8) Frangville, C.; Rutkevičius, M.; Richter, A. P.; Velev, O. D.; Stoyanov, S. D.; Paunov, V. N. Fabrication of Environmentally Biodegradable Lignin Nanoparticles. *ChemPhysChem* **2012**, *13*, 4235−4243.
(9) Munk, L.; Sitarz, A. K.; Kalyani, D. C.; Mikkelsen, J. D.; Meyer, A. S. Can Laccases Catalyze Bond Cleavage in Lignin? *Biotechnol. Adv.* **2015**, *33*, 13−24.
(10) Legras-Lecarpentier, D.; Stadler, K.; Weiss, R.; Guebitz, G. M.; Nyanhongo, G. S. Enzymatic Synthesis of 100% Lignin Biobased Granules as Fertilizer Storage and Controlled Slow Release Systems. *ACS Sustain. Chem. Eng.* **2019**, *7*, 12621−12628.
(11) Mattinen, M.-L.; Riviere, G.; Henn, A.; Nugroho, R.; Leskinen, T.; Nivala, O.; Valle-Delgado, J.; Kostiainen, M.; Österberg, M. Colloidal Lignin Particles as Adhesives for Soft Materials. *Nanomaterials* **2018**, *8*, 1001.
(12) Henn, A.; Mattinen, M.-L. Chemo-Enzymatically Prepared Lignin Nanoparticles for Value-Added Applications. *World J. Microbiol. Biotechnol.* **2019**, *35*, 1−9.
(13) Vishtal, A.; Kraslawski, A. Challenges in Industrial Applications of Technical Lignins. *BioResources* **2011**, *6*, 3547−3568.
(14) Wang, L.; Lagerquist, L.; Zhang, Y.; Koppolu, R.; Tirri, T.; Sulaeva, I.; Schoultz, S. v.; Vähäsalo, L.; Pranovich, A.; Rosenau, T.; et al. Tailored Thermosetting Wood Adhesive Based on Well-Defined Hardwood Lignin Fractions. *ACS Sustain. Chem. Eng.* **2020**, *8*, 13517−13526.
(15) Gioia, C.; Lo Re, G.; Lawoko, M.; Berglund, L. Tunable Thermosetting Epoxies Based on Fractionated and Well-Characterized Lignins. *J. Am. Chem. Soc.* **2018**, *140*, 4054−4061.
(16) Zhang, R.; Du, Q.; Wang, L.; Zheng, Z.; Guo, L.; Zhang, X.; Yang, X.; Yu, H. Unlocking the response of lignin structure for improved carbon fiber production and mechanical strength. *Green Chem.* **2019**, *21*, 4981−4987.
(17) Crestini, C.; Lange, H.; Sette, M.; Argyropoulos, D. S. On the Structure of Softwood Kraft Lignin. *Green Chem.* **2017**, *19*, 4104−4121.
(18) Liu, H.; Zhu, L.; Bocola, M.; Chen, N.; Spiess, A. C.; Schwaneberg, U. Directed Laccase Evolution for Improved Ionic Liquid Resistance. *Green Chem.* **2013**, *15*, 1348−1355.
(19) Itoh, T.; Takagi, Y. Laccase-Catalyzed Reactions in Ionic Liquids for Green Sustainable Chemistry. *ACS Sustain. Chem. Eng.* **2021**, *9*, 1443−1458.
(20) Longe, L. F.; Couvreur, J.; Leriche Grandchamp, M.; Garnier, G.; Allais, F.; Saito, K. Importance of Mediators for Lignin Degradation by Fungal Laccase. *ACS Sustain. Chem. Eng.* **2018**, *6*, 10097−10107.
(21) Liu, H.; Zhu, L.; Wallraf, A.-M.; Räuber, C.; Grande, P. M.; Anders, N.; Gertler, C.; Werner, B.; Klankermayer, J.; Leitner, W.; et al. Depolymerization of Laccase-Oxidized Lignin in Aqueous Alkaline Solution at 37 °C. *ACS Sustain. Chem. Eng.* **2019**, *7*, 11150−11156.
(22) Guan, Z.-B.; Luo, Q.; Wang, H.-R.; Chen, Y.; Liao, X.-R. Bacterial Laccases: Promising Biological Green Tools for Industrial Applications. *Cell. Mol. Life Sci.* **2018**, *75*, 3569−3592.
(23) Hämäläinen, V.; Grönroos, T.; Suonpää, A.; Heikkilä, M. W.; Romein, B.; Ihalainen, P.; Malandra, S.; Birikh, K. R. Enzymatic Processes to Unlock the Lignin Value. *Front. Bioeng. Biotechnol.* **2018**, *6*, 1−10.
(24) von Schoultz, S. Method for Extracting Biomass. WO2014009604A1, 2014.
(25) von Schoultz, S. Method for Extracting Lignin. WO2015104460A1, 2015.
(26) Baltierra-Trejo, E.; Márquez-Benavides, L.; Sánchez-Yáñez, J. M. Inconsistencies and Ambiguities in Calculating Enzyme Activity: The Case of Laccase. *J. Microbiol. Methods* **2015**, *119*, 126−131.

(27) Zhao, C.; Li, S.; Zhang, H.; Yue, F.; Lu, F. Structural Insights into the Alkali Lignins Involving the Formation and Transformation of Arylglycerols and Enol Ethers. *Int. J. Biol. Macromol.* **2020**, *152*, 411−417.
(28) Zhao, C.; Huang, J.; Yang, L.; Yue, F.; Lu, F. Revealing Structural Differences between Alkaline and Kraft Lignins by HSQC NMR. *Ind. Eng. Chem. Res.* **2019**, *58*, 5707−5714.
(29) Lagerquist, L.; Pranovich, A.; Smeds, A.; von Schoultz, S.; Vähäsalo, L.; Rahkila, J.; Kilpeläinen, I.; Tamminen, T.; Willför, S.; Eklund, P. Structural Characterization of Birch Lignin Isolated from a Pressurized Hot Water Extraction and Mild Alkali Pulped Biorefinery Process. *Ind. Crops Prod.* **2018**, *111*, 306−316.
(30) Balakshin, M. Y.; Capanema, E. A.; Chen, C. L.; Gracz, H. S. Elucidation of the Structures of Residual and Dissolved Pine Kraft Lignins Using an HMQC NMR Technique. *J. Agric. Food Chem.* **2003**, *51*, 6116−6127.
(31) Shimizu, S.; Yokoyama, T.; Matsumoto, Y. Effect of type of aromatic nucleus in lignin on the rate of the β-O-4 bond cleavage during alkaline pulping process. *J. Wood Sci.* **2015**, *61*, 529−536.
(32) Li, S.; Lundquist, K.; Westermark, U. Cleavage of syringylglycerol ß-syringyl ethers during soda cooking. *Nord. Pulp Pap. Res. J.* **2000**, *15*, 205−210.
(33) Huber, D.; Pellis, A.; Daxbacher, A.; Nyanhongo, G.; Guebitz, G. Polymerization of Various Lignins via Immobilized Myceliophthora Thermophila Laccase (MtL). *Polymers* **2016**, *8*, 280.
(34) Chan, J. C.; Paice, M.; Zhang, X. Enzymatic Oxidation of Lignin: Challenges and Barriers Toward Practical Applications. *ChemCatChem* **2020**, *12*, 401−425.
(35) Dizhbite, T.; Telysheva, G.; Jurkjane, V.; Viesturs, U. Characterization of the radical scavenging activity of lignins??natural antioxidants. *Bioresour. Technol.* **2004**, *95*, 309−317.
(36) Meng, X.; Crestini, C.; Ben, H.; Hao, N.; Pu, Y.; Ragauskas, A. J.; Argyropoulos, D. S. Determination of hydroxyl groups in biorefinery resources via quantitative 31P NMR spectroscopy. *Nat. Protoc.* **2019**, *14*, 2627−2647.
(37) Dongre, P.; Driscoll, M.; Amidon, T.; Bujanovic, B. Lignin-Furfural Based Adhesives. *Energies* **2015**, *8*, 7897−7914.
(38) Camarero, S.; Galletti, G. C.; Martínez, A. T. Demonstration ofIn Situ Oxidative Degradation of Lignin Side Chains by Two White-rot Fungi Using Analytical Pyrolysis of Methylated Wheat Straw. *Rapid Commun. Mass Spectrom.* **1997**, *11*, 331−334.
(39) Jiang, Y.; Liu, X.; Yang, Q.; Song, X.; Qin, C.; Wang, S.; Li, K. Effects of Residual Lignin on Mechanical Defibrillation Process of Cellulosic Fiber for Producing Lignocellulose Nanofibrils. *Cellulose* **2018**, *25*, 6479−6494.
(40) Wang, Q.; Du, H.; Zhang, F.; Zhang, Y.; Wu, M.; Yu, G.; Liu, C.; Li, B.; Peng, H. Flexible cellulose nanopaper with high wet tensile strength, high toughness and tunable ultraviolet blocking ability fabricated from tobacco stalk via a sustainable method. *J. Mater. Chem. A* **2018**, *6*, 13021−13030.
(41) Farooq, M.; Zou, T.; Riviere, G.; Sipponen, M. H.; Österberg, M. Strong, Ductile, and Waterproof Cellulose Nanofibril Composite Films with Colloidal Lignin Particles. *Biomacromolecules* **2019**, *20*, 693−704.
(42) Pasquier, E.; Mattos, B. D.; Belgacem, N.; Bras, J.; Rojas, O. J. Lignin Nanoparticle Nucleation and Growth on Cellulose and Chitin Nanofibers. *Biomacromolecules* **2020**, *22*, 880−889.

https://doi.org/10.1021/acssuschemeng.1c01576
ACS Sustainable Chem. Eng. 2021, 9, 8770−8782